Journal of Bionic Engineering
https://doi.org/10.1007/s42235-022-00251-8

RESEARCH ARTICLE

Properties of Collagen/Sodium Alginate Hydrogels for Bioprinting of Skin Models

Tian Jiao[1] · Qin Lian[1,2] · Weilong Lian[1] · Yonghui Wang[1] · Dichen Li[1] · Rui L. Reis[3,4] · Joaquim Miguel Oliveira[3,4]

Received: 21 January 2022 / Revised: 15 July 2022 / Accepted: 21 July 2022

Abstract
3D printing technology has great potential for the reconstruction of human skin. However, the reconstructed skin has some differences from natural skin, largely because the hydrogel used does not have the appropriate biological and physical properties to allow healing and regeneration. This study examines the swelling, degradability, microstructure and biological properties of Collagen/Sodium Alginate (Col/SA) hydrogels of differing compositions for the purposes of skin printing. Increasing the content of sodium alginate causes the hydrogel to exhibit stronger mechanical and swelling properties, a faster degradation ratio, smaller pore size, and less favorable biological properties. An optimal 1% collagen hydrogel was used to print bi-layer skin in which fibroblasts and keratinocytes showed improved spreading and proliferation as compared to other developed formulations. The Col/SA hydrogels presented suitable tunability and properties to be used as a bioink for bioprinting of skin aiming at finding applications as 3D models for wound healing research.

Keywords Bioink · Bioprinting · Collagen/sodium alginate hydrogel · Skin · Wound healing · Bionic

1 Introduction

Skin is the largest human organ [1] and has many vital functions, including protection against pathogens and UV-light [2, 3], sensing of the external environment, regulation of body temperature and excretion of waste [4]. Extensive skin damage increases the risk of wound infection and the resulting disorder of immune function and metabolism may cause shock or even death [5, 6]. The World Health Organization reports that about 300,000 people die every year due to severe skin trauma [7], illustrating the urgent need for skin substitutes that can be used for clinical transplantation.

Wound dressings provide temporary cover for skin injuries but do not promote regeneration. By contrast, various skin substitutes are available, including those produced by tissue culture, which does promote wound healing [8, 9]. However, the use of foreign cells still has the risk of immune rejection and disease transmission [10]. In addition, tissue-engineered skin cannot fit the different shapes and depths of individual wounds [11]. 3D bioprinting can be used to build complex tissues via a process of depositing cells and extracellular matrix layer by layer [12–14] and is reproducible, easily standardized and highly efficient [15, 16].

Over the past two decades, 3D bioprinting using hydrogels containing skin cells has been used to create increasingly complex models of skin [17–21]. The dermis was initially constructed [22–24], followed by a bi-layer (epidermis and dermis) [25–29] and tri-layer (epidermis, dermis and subcutaneous tissue) [21, 30, 31], as the structure of the printed skin became a closer approximation of natural skin. Initially, fibroblasts and keratinocytes were used [28, 32, 33], with the later addition of endothelial cells and melanocytes to reconstruct blood vessels and impart color [34–37]. Although printed skin is functionally similar to human skin [15, 16] and has been shown to promote the repair of animal skin wounds [25, 33],

✉ Qin Lian
lqiamt@mail.xjtu.edu.cn

1 State Key Laboratory for Manufacturing System Engineering, Xi'an Jiaotong University, Xi'an 710049, China

2 Shaanxi Ketao-AM Technology Co., Ltd., Xi'an 710100, China

3 3B's Research Group, I3Bs—Research Institute on Biomaterials, Biodegradables and Biomimetics, Headquarters of the European Institute of Excellence on Tissue Engineering and Regenerative Medicine, University of Minho, Barco, 4805-017 Guimarães, Portugal

4 ICVS/3B's–PT Government Associate Laboratory, Barco, 4805-017 Guimarães, Portugal

Published online: 07 September 2022

scarring is an inevitable byproduct of the healing process [31, 33, 38], as the reconstructed skin has some mechanical and biological differences from the surrounding natural skin [39, 40].

The mechanical properties, microstructure, degradability and biological properties of transplanted skin determine its role in the process of skin healing and reconstruction [10, 41, 42]. An appropriate hydrogel is central to successful healing. The hydrogel must have sufficient cell attachment ligands (> 200 μm) to facilitate cell adhesion and proliferation [43]. In addition, the pore size (20–125 μm) must be suitable to allow the growth of small cell colonies, thereby avoiding the formation of scar tissue due to directional collagen fibers [43, 44]. The hydrogel degradation half-life (14 ± 7 days) should coincide with the timescale of skin reconstruction [43, 45] and its mechanical properties should reflect those of the surrounding skin tissue.

Hydrogels used for skin printing usually include collagen, gelatin, sodium alginate, fibrinogen, hyaluronic acid and chitosan [46, 47]. Collagen hydrogels have many of the cell attachment ligands required for cell adhesion and proliferation but have poor mechanical properties [43, 48]. By contrast, gelatin hydrogels are temperature-sensitive with few cell attachment ligands and lower bioactivity relative to collagen [46]. The sodium alginate used for hydrogel construction is non-toxic and has no bioactivity [49]. Through cross linkages with divalent metal ions, it forms a hydrogel with favorable mechanical properties and which maintains printing structure [12]. Fibrinogen hydrogels are easily crosslinked in the presence of thrombin and have excellent bioactivity and degradation properties [50, 51]. Combining these different components is the route to optimization of hydrogel properties.

The biological and physical properties of 3D printed skin play a critical role in wound healing and skin reconstruction. Only with a suitable swelling rate, degradation rate, mechanical properties, pore size, and cell attachment sites for hydrogels used for skin printing can be the reconstructed skin structure and function be closer to natural skin. This study proposes blending collagen and sodium alginate to obtain hydrogels with excellent mechanical and biological properties. The swelling, degradability, mechanical properties, microstructure and biological properties of different formulations Col/SA hydrogels were tested and analyzed according to the need for the hydrogel properties for wound healing and skin reconstruction. The optimally formulated Col/SA hydrogel was selected for bi-layer skin printing and evaluation.

2 Materials and Methods

2.1 Materials

Sodium alginate(A2033) and sodium hydroxide (71,687) were purchased from Sigma-Aldrich. Ultra-pure water (18.2 MΩ cm, < 10 CFU/ml) was distilled in the laboratory. Acetic acid (A801299) was purchased from Macklin. 10 × Dulbecco's Modified Eagle Medium (DMEM) powders (1012800-017), fetal bovine serum (10,270–106) and Penicillin/Streptomycin mixed solution (15140-122) were purchased from Gibco. DMEM (SH30022), Iscove's Modified Dulbecco's Medium (IMDM, SH30228) and Phosphate Buffer Saline (PBS, SH30256) were purchased from Hyclone. Cell-tracker green (C2925) and cell-tracker red (C1046) were purchased from Thermo Fisher Scientific.

2.2 Preparation of Collagen

We extracted type I rat tail collagen according to Rittie's method [52]. Sixteen adult Sprague–Dawley (SD) rats were purchased from the Animal Experimental Center of Xi'an Jiaotong University. All experiments had been approved by the Institutional Animal Care and Use Committee of the Ethics Committee of Xi'an Jiaotong University Health Science Center, China. Tails of adult SD rats were soaked in 75% alcohol for 24 h and the skin was stripped. Tail bones were broken off section by section and the tendon was extracted and cut into pieces. The tendon was dissolved in 0.1% (*v*/*v*) acetic acid solution at 1 g/500 ml. The collagen solution was stirred at 200 rpm for 48 h using an electric stirrer (XREM-100 s, Xinrui Instrument Factory) followed by centrifugation at 5000 rpm for the period of 2 h and at 4 °C. The supernatant was frozen in a sterile tinfoil box (solution height < 10 mm) at − 80 °C for 24 h before freeze-drying for 72 h to obtain collagen foam. The above steps were performed under sterile, low-temperature conditions to avoid contamination or gelation of collagen.

2.3 Cell Culture

Normal Human Dermal Fibroblasts (NHDFs, purchased from American Type Culture Collection) were cultured in a medium of fetal bovine serum, Penicillin/Streptomycin mixture and DMEM in a volume ratio of 10:1:89. Normal Human Epidermal Keratinocytes (NHEKs, purchased from American Type Culture Collection) were cultured in a medium of fetal bovine serum, Penicillin/Streptomycin mixture and IMDM in a volume ratio of 10:1:89. Cells were cultured at 37 °C with 5% CO_2 in air. The culture

medium was changed daily and passage was performed at 70% confluence.

2.4 Preparation of Bioinks

Chopped collagen foam was dissolved in 0.1% (*v*/*v*) acetic acid solution, previously dissolved at 4 °C for 48 h, to a concentration of 2.5% or 5% (*w*/*v*). Sodium alginate was sterilized at 121 °C for 30 min before being dissolved in sterile ultrapure water to a concentration of 1.25%, 2.5%, 5% or 10% (*w*/*v*) by placing in a 50 °C water bath for 24 h. The 2 M sodium hydroxide and 10 × DMEM powders were dissolved in sterile ultrapure water, respectively. All the above solutions were chilled in a refrigerator at 4 °C for 4 h. 1 ml of collagen solution and 1 ml of sodium alginate solution were mixed and 2 ml of the Col/SA solution blended with 0.25 ml of 10 × DMEM solution and 25 µl of sodium hydroxide solution added. Fibroblasts and keratinocytes were labeled with cell-tracker green and cell-tracker red, respectively, and 0.25 ml of a 10^7 cells/ml suspension of each cell type was used to prepare bioinks. An aseptic environment below 10 °C with low light was employed throughout. Several Col/SA bioinks formulations (10 groups) were prepared with different proportions of collagen and sodium alginate. Compositions are shown in Table 1. C and A represent the content of collagen and sodium alginate in the respective hydrogels. Cell-free inks were prepared as described above but without adding the cell and used for physical property tests.

2.5 Rheological Analysis

Rheological analysis of Col/SA bioink was performed using a rotational rheometer (HR2, TA Instruments, USA). A 20 mm diameter plate was used for shear rate (0.1 ~ 100 rad/s, 10 °C) and time (0 ~ 1800 s, 37 °C, frequency 10 Hz) analysis to measure the viscosity, the storage modulus (G') and loss modulus (G'').

2.6 Bioprinting Hydrogel Structures

A temperature-controlled extrusion bioprinter was constructed and used to print Col/SA hydrogel structures. Printing parameters were set as follows: 25G (260 µm) printhead; 10 °C ink temperature; 0.2 ml/minute ink extrusion flow; 15 mm/s printhead movement speed. Various sizes of hydrogel were printed using the Col/SA bioinks and 15 mm × 15 mm × 1 mm structures were used to evaluate swelling and degradation properties. Cylindrical hydrogel structures of 10 mm diameter × 10 mm height were printed to evaluate compression properties and 100 mm × 20 mm × 1 mm structures to evaluate tensile properties. Fibroblasts-containing structures of 15 mm × 15 mm × 0.5 mm were printed to evaluate biological properties. All printed hydrogel structures were immersed in sterile 3% calcium chloride solution at 37 °C for 5 min to facilitate sodium alginate crosslinking and then incubated at 37 °C for 0.5 h to facilitate collagen gelation.

2.7 Swelling Test

Hydrogel structures were soaked in PBS at 37 °C for 0, 0.5, 1.5, 3, 6, 9 and 24 h before draining of superficial solution and weighing. The swelling rate of Col/SA hydrogel was calculated by Amirian's method, as shown in Eq. (1) [53]. The ratio of the increased hydrogel mass after immersion to initial mass constitutes the swelling ratio.

$$\text{Swelling ratio } (\%) = \frac{W_t - W_0}{W_0} \times 100, \tag{1}$$

where W_t was the weight of swollen sample at a predetermined time, and W_0 was the initial weight.

2.8 Degradation Test

Hydrogel structures were soaked in PBS at 37 °C for 0, 1, 4, 7, 10 and 14 days, freeze-dried for 48 h and weighed. The degradation rate of Col/SA hydrogel was calculated by Zhang's method, as shown in Eq. (2) [54]. The ratio of the hydrogel mass to the initial mass constitutes the degradation ratio.

$$\text{Degradation ratio } (\%) = \frac{W_{d0} - W_{dt}}{W_{d0}} \times 100, \tag{2}$$

where W_{dt} was the dry weight of the degradation sample at a predetermined time, and W_{d0} was the initial dry weight.

2.9 Compression and Tensile Test

Hydrogels were tested for compression and tensile properties using a six-channel material mechanics testing machine (Prosim, UK) according to Chinese compression and tensile test standards (GB/T 1488–2005 and GB/T 1040.3–2006).

Table 1 Formulation of the Col/SA bioinks

Formulation	C1	C1A0.5	C1A1	C1A2	C1A4	C2	C2A0.5	C2A1	C2A2	C2A4
Col content (w/v)	1%	1%	1%	1%	1%	2%	2%	2%	2%	2%
SA Content(w/v)	0%	0.5%	1%	2%	4%	0%	0.5%	1%	2%	4%
Cell density	10^6 cells/ml fibroblasts or keratinocytes									

The gauge length for compression and tensile tests is set to 10 mm and 60 mm, respectively. Strain, compression modulus, tensile modulus and elongation at break were calculated by the software of the mechanical experiment machine.

2.10 Scanning Electron Microscope (SEM) Characterization

After freeze-drying for 48 h, cross-section morphology of hydrogels was photographed by field emission scanning electron microscope (Nikon SU8000, Japan). We used the software ImageJ to extract the pores and calculate the pore area, and then the pore size (diameter) was calculated by the area formula of the circle.

2.11 Evaluation of Biological Properties

Hydrogels containing green fluorescently labeled NHDFs were immersed in NHDF medium and cultured at 37 °C with 5% CO_2 for one week with a daily medium change. The morphology and distribution of NHDFs were observed using a laser confocal microscope (Nikon A1, Japan) on days 1, 3, 5 and 7 after printing. Cell numbers and proliferation ratios were calculated for different hydrogel compositions and at different time points.

2.12 Bioprinting and Evaluation of Bi-layer Skin

Two layers of 1% (*w*/*v*) collagen hydrogel containing fibroblasts were extruded and printed to constitute the dermis, followed by a superficial layer of 1% (*w*/*v*) collagen ink containing keratinocytes to constitute the epidermis (Fig. 1). The resulting structures were cultured in a 37 °C with 5% CO_2 for three days with daily medium changes. Morphology and distribution of NHDFs and NHEKs were observed by confocal laser microscopy (Nikon A1, Japan) at days 1 and 3 after printing.

2.13 Statistical Analysis

All experiments were performed, at least, in quintuplicate, and the obtained results were presented as average ± SD (standard deviation). The standard *t* test was carried out to compare the statistical significance between the two groups (*$p < 0.05$, **$p < 0.01$, and ***$p < 0.001$), which was statistically significant.

3 Results and Discussion

3.1 Rheology of Bioink

We evaluated printability by measuring the viscosity change as a function of shear rate (0. 1 ~ 100 rad/s) at 10 °C (Fig. 2a, b). The results showed that the viscosity of the bioink increased with the content of collagen and sodium alginate. It was also observed that all of the bioinks exhibited a linear decrease in viscosity with increasing shear rate, indicating that Col/SA bioink were non-Newtonian fluids with shear-thinning properties at different concentrations. Thus, all concentrations Col/SA bioink can be extruded smoothly through a nozzle without clogging [11, 25]. To understand the gelation process of Col/SA hydrogels, we tested the changes of storage modulus (G') and loss modulus (G'') of the hydrogels at 37 °C for 30 min (Fig. 2c, d). G' and G'' of all Col/SA bioink stabilized at 30 min, and G' was higher than G''. The

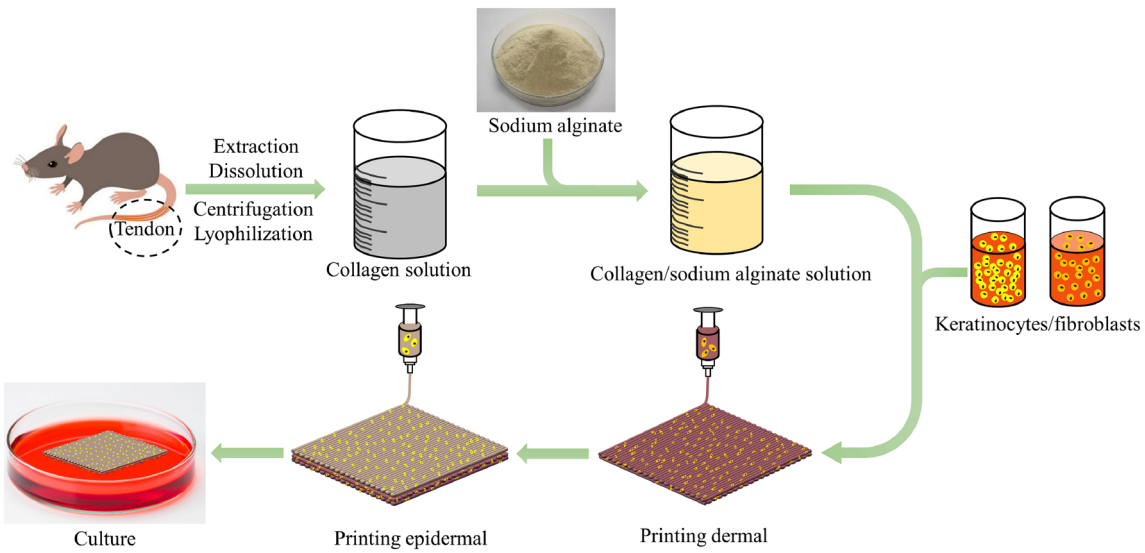

Fig. 1 Schematic diagram of bioink preparation and skin printing

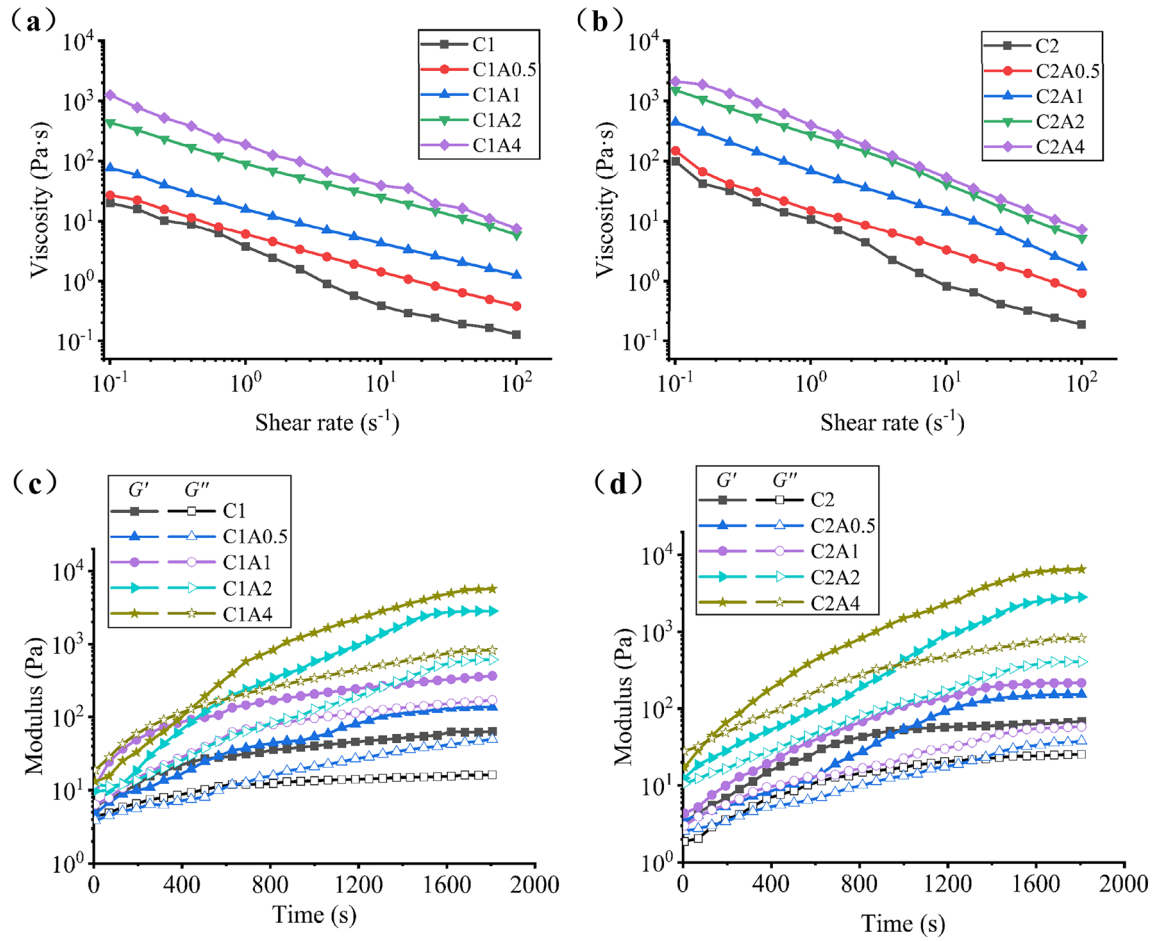

Fig. 2 Rheological properties of bioink: **a**, **b** Viscosity of bioink at 0.1 s^{-1}–100 s^{-1} shear rate at 4 °C; **c**, **d** Storage modulus (*G′*) and loss modulus (*G″*) of bioinks at 37 °C for 30 min

results show that all concentrations of Col/SA inks can be crosslinked within 30 min. As the content of sodium alginate or collagen in the bioink increases, the difference between *G′* and *G″* is larger. The results show that increasing the content of sodium alginate and collagen in the bioink can improve the stability and mechanical strength of the printed hydrogel structure [11, 55].

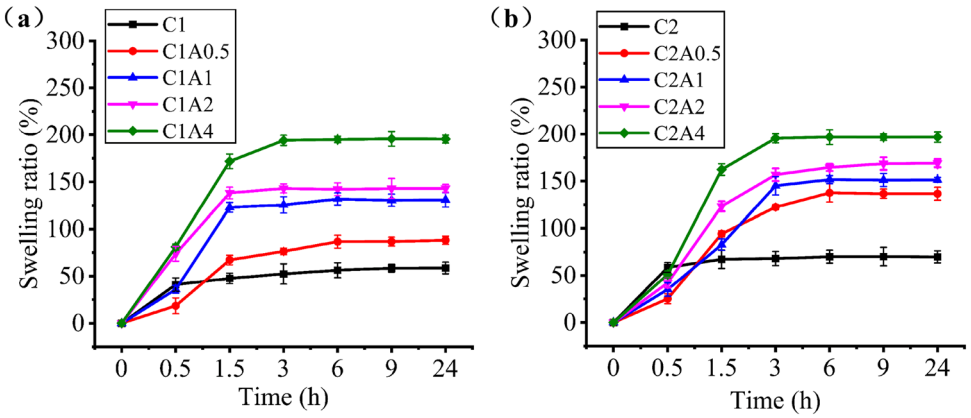

Fig. 3 Swelling ratios of Col/SA hydrogels up to 24 h of soaking

3.2 Swelling Properties of Hydrogel

Swelling ratios are shown in Fig. 3. Swelling ratios tended to increase with soaking time up to a maximum of 3 h. The greatest increase for C1 and C2 hydrogels was seen during the first 0.5 h of soaking and, for other hydrogels, during the first 3 h of soaking. The swelling mechanism for hydrogel with a pore size in the range of several hundred micrometers is based on the capillary force. The hydrogel can quickly reach the swelling equilibrium in a relatively short duration [53]. Comparison of the 24 h swelling ratio revealed a proportionality to sodium alginate content with the value for C2A4 being more than 3 times that of C1 (Table 2). Values for 2% collagen hydrogels were higher than those for 1% collagen hydrogels (Table 2).

During the first 1.5 h (0.5 h for C1 and C2), the external liquid quickly diffused through the micropores to make hydrophilic bonds within the hydrogel, leading to a rapid increase in swelling ratio. At 1.5 to 3 h, the pores were fluid-filled and the hydrogel gradually became saturated, slowing the increase in swelling ratio. After 3 h, the hydrogels were completely saturated and the swelling ratio did not change significantly. As can be seen from Fig. 3, the C1 and C2 hydrogels absorbed water quickly due to their large pore size but had a lower absorption capacity. Hydrogels with higher sodium alginate or collagen content had more hydrophilic bonds to increase capacity, giving higher swelling ratios. Excellent swelling capacity is one of the vital properties which can provide a moist environment for wound healing and skin reconstruction [56, 57]. For the purposes of printing skin, a higher swelling ratio is more conducive to infiltration of culture medium or tissue fluid around the transplanted skin which promotes cell growth, proliferation and tissue maturation [54]. Analysis of swelling ratios reveals that hydrogels with higher sodium alginate or collagen content are more suitable for skin printing.

3.3 Degradability of Hydrogel

Figure 4 shows degradation photos for Col/SA hydrogels soaked in PBS at 37 °C up to 14 days. By means of weighing

Table 2 Swelling ratios of Col/SA hydrogels after 24 h of soaking

Formulation	C1	C1A0.5	C1A1	C1A2	C1A4	C2	C2A0.5	C2A1	C2A2	C2A4
Swelling ratio	58.8	88.3	131.0	143.2	195.5	69.8	136.7	151.3	169.1	196.8

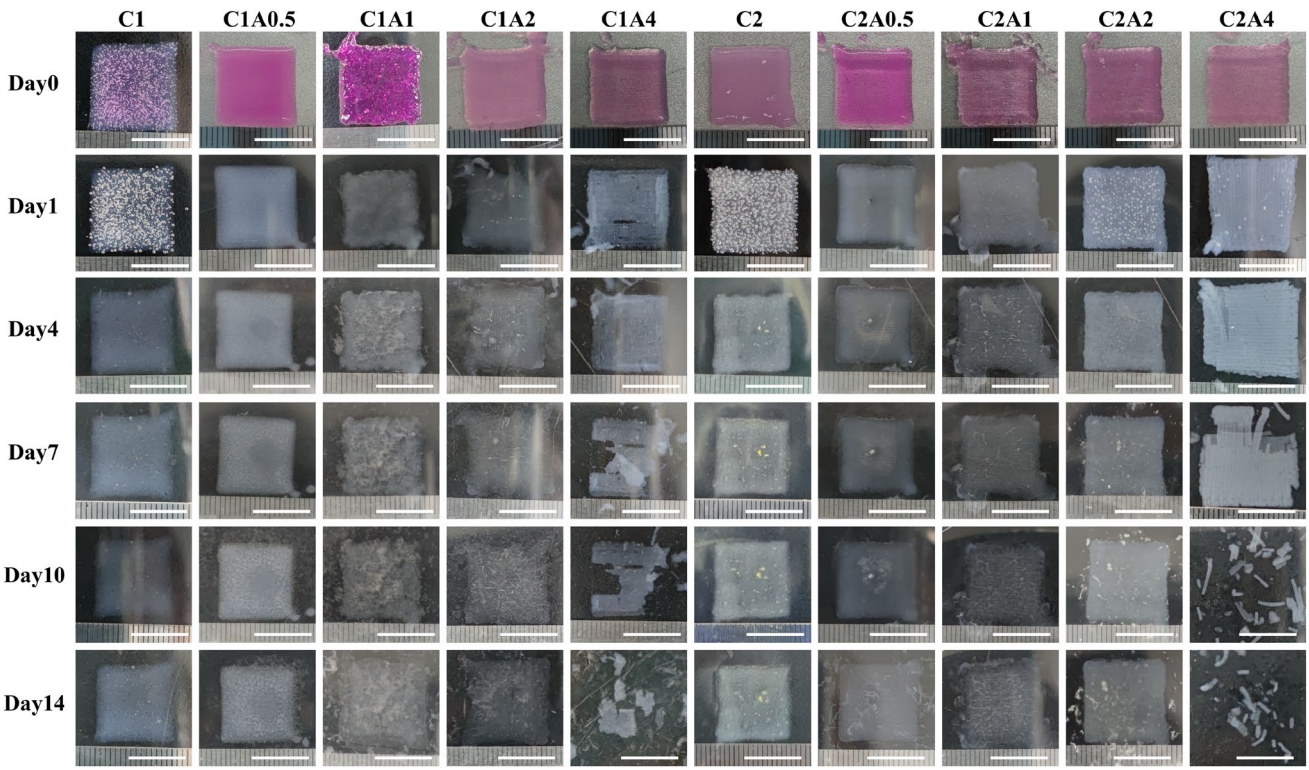

Fig. 4 Photographs of Col/SA hydrogels after soaking in PBS for the period of 14 days (scale bar: 10 mm)

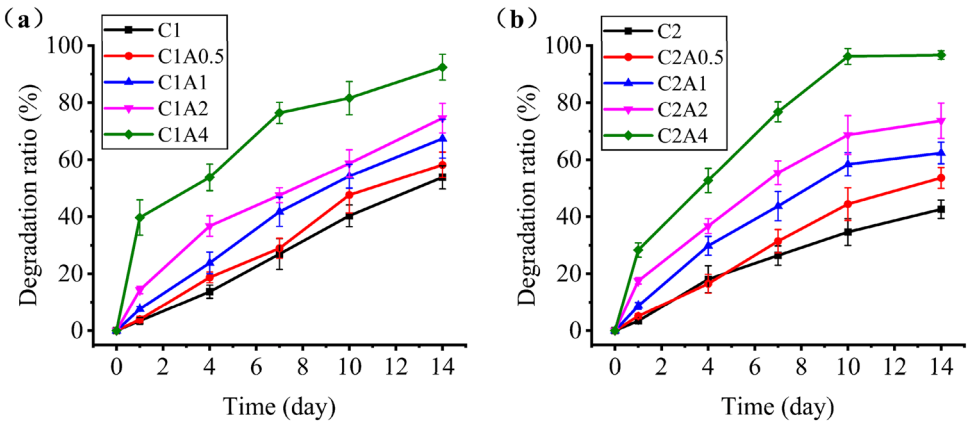

Fig. 5 Degradation ratios of Col/SA hydrogels after soaking in PBS for the period of 14 days

Table 3 Degradation ratios of Col/SA hydrogel at day 14

Formulation	C1	C1A0.5	C1A1	C1A2	C1A4	C2	C2A0.5	C2A1	C2A2	C2A4
Degradation ratio	53.8	58.2	67.4	74.6	92.4	42.6	53.6	62.4	73.7	96.7

hydrogels at different time points, degradation ratio changes (Fig. 5), including the day 14 timepoint (Table 3) after which little size change was observed, were calculated. No obvious hydrogel shrinkage was observed with only C2A4 showing significant bloating. Shrinkage of transplanted printed skin around the wound site is likely to lead to scar formation and should be avoided. Col/SA hydrogels show minimal shrinkage, making them suitable for skin printing.

Figures 4 and 5 show that Col/SA hydrogels show gradual degradation in proportion to immersion time. Degradation ratios were between 42.6 and 96.7%. Uniform degradation of the C1, C1A0.5, C1A1, C1A2 and C2 hydrogels occurred throughout the experimental period. C2A0.5, C2A1 and C2A2 hydrogels degraded uniformly over the first 10 days before degradation slowed. C1A4 and C2A4 degraded very quickly during the first day and thereafter degraded slowly. Increasing the content of sodium alginate resulted in more rapid degradation.

In general, as the sodium alginate concentration in the hydrogel increases, the hydrogel will have more crosslinking sites, resulting in a decreased degradation rate [58]. However, different results appeared in this experiment, and the main reason is probably that hydrolysis accelerated the degradation of the hydrogel. From the swelling test results of the hydrogel, it was found that the swelling ratio of the Col/SA hydrogel increased with the increase of the sodium alginate content. The hydrolysis of the hydrogel is accelerated by increasing of absorption water in the hydrogel, which can break more covalent bonds in the hydrogel and lead to rapid degradation of the hydrogel [53].

If the transplanted skin cannot be degraded, it will cause long-term inflammation [59]. The ideal biomaterial scaffold for tissue engineering should have an equal degradation rate along with new tissue regeneration [60]. Previous studies have shown a degradation half-life of 14 ± 7 days to be optimal for cell growth and skin wound repair by transplantation of printed skin [43–45]. This equates to a 50% degradation ratio after 14 days for a hydrogel to be suitable for skin printing. C1 and C2A0.5 hydrogels show the most favorable degradation ratios of those tested (Table 3). Lower degradation ratios of the C2 hydrogel will not adequately support cell migration and tissue reconstruction and higher degradation ratios of C1A4 and C2A4 will not provide sufficient support and protection to allow wound reconstruction.

3.4 Mechanical Properties of Hydrogel

Compression experiments were performed on hydrogels of 10 mm diameter and 10 mm height using a mechanical testing machine (Fig. 6a). Compression modulus are shown in Fig. 6c. With increasing sodium alginate content, the C1 compression modulus increased from 15.6 to 35.9 kPa and that of C2 increased from 20.5 to 38.0 kPa. Compression modulus for the C2 group were higher than those for the C1 group. Thus, increasing the collagen or sodium alginate content produces a corresponding increase in the compression modulus of the hydrogel. The C2A4 hydrogel had the highest compression modulus (38.0 kPa).

Comparison with previous studies revealed that the Col/SA hydrogel had a higher compression modulus (38.0 kPa) than that reported for the sodium alginate/methylcellulose hydrogel (11.11 kPa) [61] and was similar to that of the GelMA/sodium alginate hydrogel (38.5 kPa) [62]. The Col/SA hydrogel is considered to have excellent compression properties.

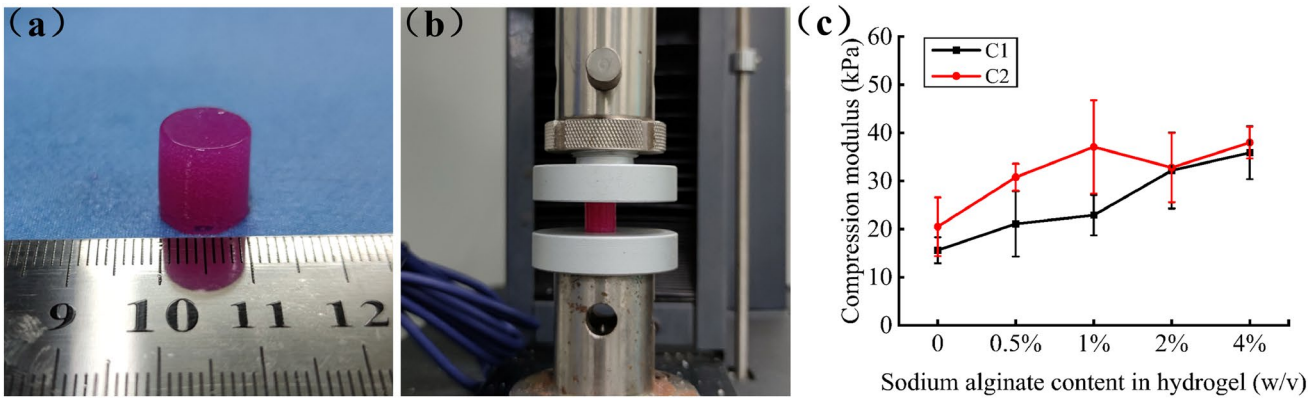

Fig. 6 Col/SA hydrogel compression test: **a** Test sample; **b** Test process; and **c** Compression modulus

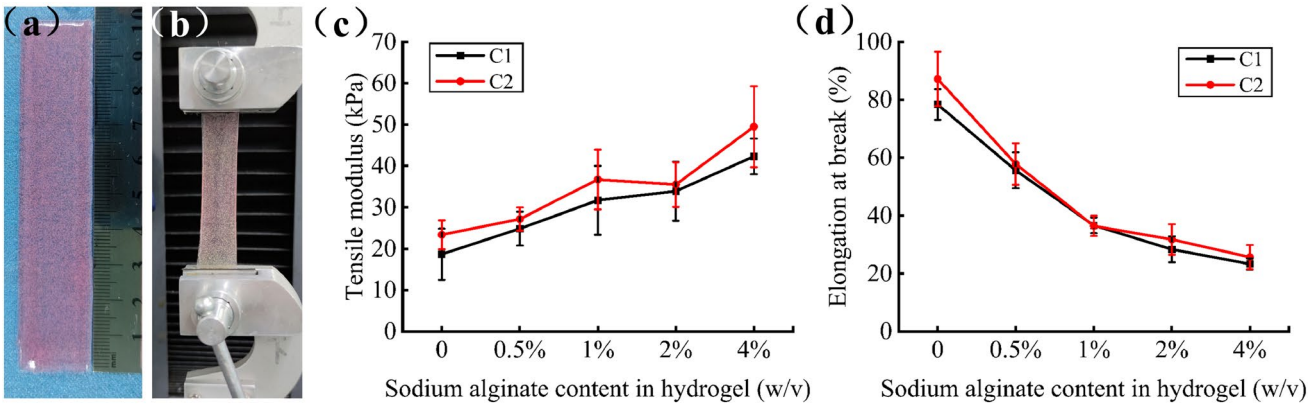

Fig. 7 Col/SA hydrogel tensile test: **a** Test sample; **b** Test process; **c** Tensile modulus; and **d** Elongation at break

An example of the Col/SA hydrogel tensile test is shown in Fig. 7a and tensile modulus in Fig. 7c. With increasing sodium alginate content, the C1 tensile modulus increased from 18.7 to 42.3 kPa and that of the C2 group from 23.4 to 49.5 kPa. The tensile modulus of the 2% collagen hydrogel was higher than that of the 1% collagen hydrogel. Thus, increasing the content of collagen and sodium alginate increases the tensile modulus of the hydrogel. The highest value for tensile modulus was shown by the C2A4 hydrogel (49.5 kPa).

Elongation ratios at tensile fracture are shown in Fig. 7d. Increasing content of sodium alginate was associated with decreased elongation at break. The elongation at break of the 2% collagen was superior to that observed for the 1% collagen hydrogel with constant sodium alginate content.

In summary, increasing the contents of sodium alginate and collagen increases the compression and tensile modulus of the hydrogels. However, increasing sodium alginate content reduced the elongation at break. The denser hydrogels resulting from higher sodium alginate and collagen content more successfully resist compression and support tensile loads. However, sodium alginate prevents some interactions between collagen fibers resulting in a hydrogel which does not sustain elongation. We compared Col/SA hydrogel, sodium alginate/methylcellulose hydrogel GelMA/sodium alginate hydrogel and human skin tissue [61–63]. We found that the mechanical properties of Col/SA hydrogels are at a higher level among current hydrogels, but they are significantly inferior to the mechanical properties of human skin.

3.5 Microstructure of Hydrogel

Figure 8 shows scanning electron microscope images of Col/SA hydrogels after freeze drying revealing the distribution of a large number of pores. Distribution range and average pore size are shown in Fig. 9. Increasing the content of sodium alginate or collagen caused the pore size to decrease, accounting for the improvement in the mechanical properties of compression and tension and resulting in a denser hydrogel. Abundant pores facilitate the permeation of cell culture fluid and provide space for cell growth. Previous studies have identified a pore size of 20–125 μm as optimal

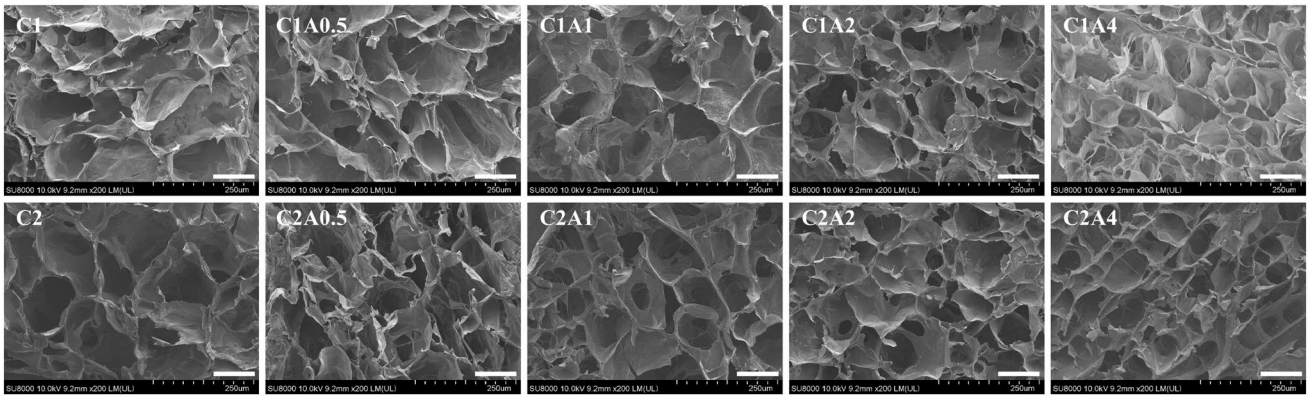

Fig. 8 SEM images of Col/SA hydrogel (scale bar: 100 μm)

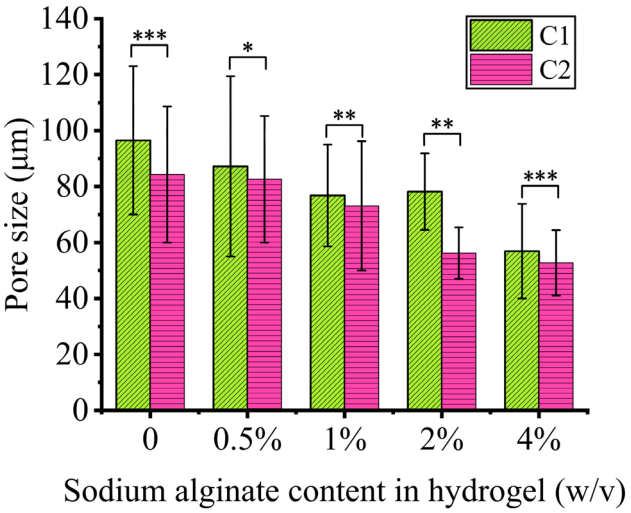

Fig. 9 Pore size of Col/SA hydrogel. $*p<0.05$, $**p<0.01$, and $***p<0.001$

for cell attachment [43]. During the process of skin healing, myofibroblasts adhere to pores of 20–125 μm and form non-directional arrangements which avoid scar formation [44, 45]. The Col/SA hydrogel presented in the current study has microscopic pores conducive to single cell attachment for the avoidance of scar formation during skin healing.

3.6 Biological Properties of Hydrogel

NHDFs were encapsulated in all hydrogels. During the process of cell culture, hydrogels C1A2, C1A4, C2A2 and C2A4 underwent significant degradation leading to the loss of cells during medium changes. No results relating to the biological properties of the hydrogels could be obtained for these groups.

Fibroblasts encapsulated into the C1 hydrogel had spread extensively after 3 days of culture and, by day 5, had formed long fibrous shapes with continuous proliferation meaning that most cells were long and fibrous by day 7 (Fig. 10). Thus, C1 provides a suitable environment for fibroblast growth and proliferation. Fibroblasts gradually proliferated within the C1A0.5 hydrogel with limited spreading by day 5 which had increased by day 7. Fibroblast proliferation was much slower within the C2 hydrogel throughout the experimental period and there was little cell spreading. No obvious cell proliferation and cell spreading were observed in the hydrogels of the C1A1, C2A0.5 and C2A1 groups.

Figure 11 shows proliferation ratios. The C1 hydrogel cell proliferation ratio increased significantly during culture, reaching 354.4% on day 7. Cell proliferation ratios for other hydrogels increased slowly with decreases becoming apparent by the 3rd or 5th day.

There are three necessary conditions for cells to survive, spread, and proliferate in the printed hydrogel. First, the hydrogel should have enough ligands for cell integrins α1β1 and α2β1 attachment [45]. Second, the hydrogel should not be too stiff or pores too small for cell spreading. Third, ink preparation, printing, and crosslinking processes cannot affect cell survival. The C1 group satisfied all the above conditions, fibroblasts showed good spreading morphology and a high proliferation rate on the 7th day after printing in C1 group. In other groups, due to the increase in the ink concentration, the hydrogel becomes harder, and the pore size becomes smaller. It is difficult to supply the culture medium and oxygen to the cells, and the growth space of the cells is limited. So the cells cannot spread and proliferate. Therefore, except for the C1 group, the cells in other groups did not show obvious spreading and proliferation. Similar results can observation in Osidak's study [64]. The proliferation ratio and survival ratio of cells in collagen hydrogel decreased significantly with increasing collagen concentration. If the extracted collagen lacks cell attachment ligands, cells cannot spread even in low concentrations (10 mg/ml) of collagen [65]. In brief, the C1 hydrogel exhibited excellent

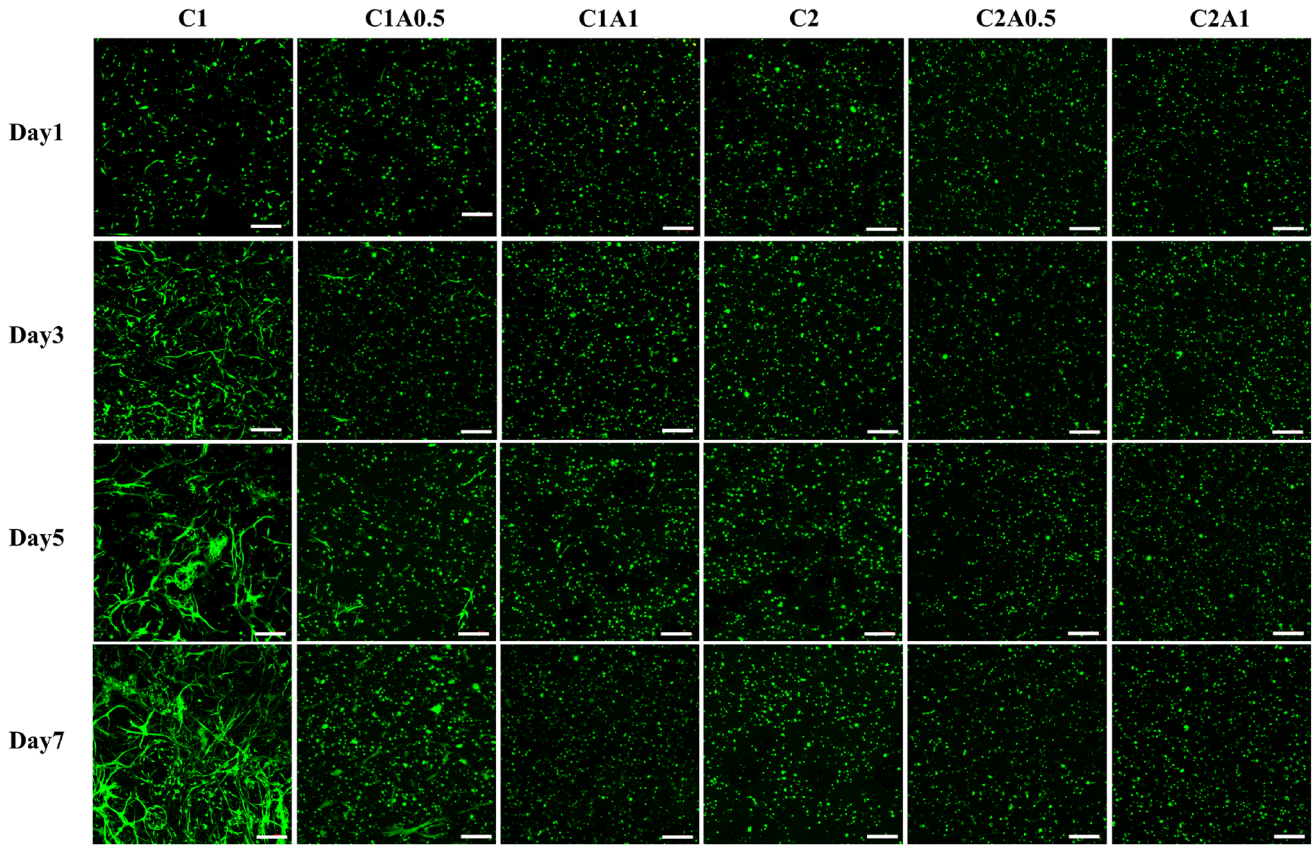

Fig. 10 Morphology and distribution of NHDFs in Col/SA hydrogels (scale bar: 200 μm)

properties in what concerns cell cytocompatibility, as it supported cell spreading and proliferation, with favorable conditions for maintaining cells functions.

The current study has analyzed and compared the properties, including degradative, swelling, mechanical, biological and pore size, of Col/SA hydrogels of differing compositions. The degradation ratio, swelling ratio, compression modulus and tensile modulus were found to increase with increasing sodium alginate content. Pore size, tensile elongation at break and cell proliferation ratio all decreased with increasing sodium alginate content. The C1 hydrogel was closest to the optimal degradation half-life (14 days) for artificial skin used for wound repair and thus best meets the needs of skin printing. The C1 hydrogel also had more favorable properties in terms of its elongation at break and cell spreading and proliferation ratio. Although increasing sodium alginate content improves the swelling ability and mechanical properties of a hydrogel, these advantages are negated by excessively fast degradation and poor biological properties. The outcome of the present study is that the C1 hydrogel is the most suitable for use in skin printing ink.

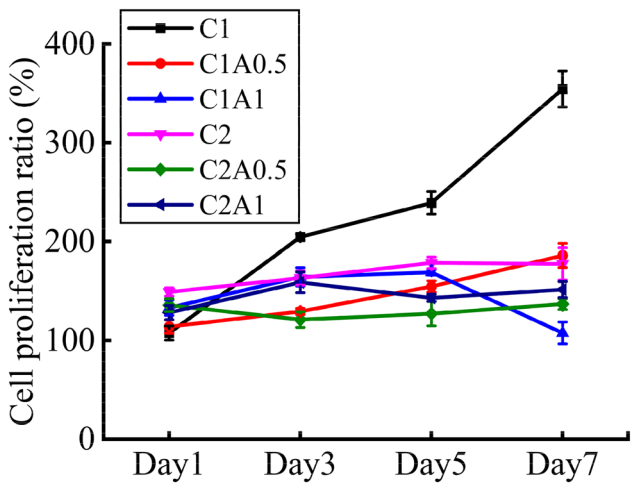

Fig. 11 Proliferation ratios of NHDFs in Col/SA hydrogels

3.7 Evaluation of Bi-layer Skin

An artificial dermis was printed using C1 hydrogel with green fluorescent labeled fibroblasts followed by a second layer with red fluorescent labelled keratinocytes to form the epidermal layer. Printed bi-layer skin was cultured for

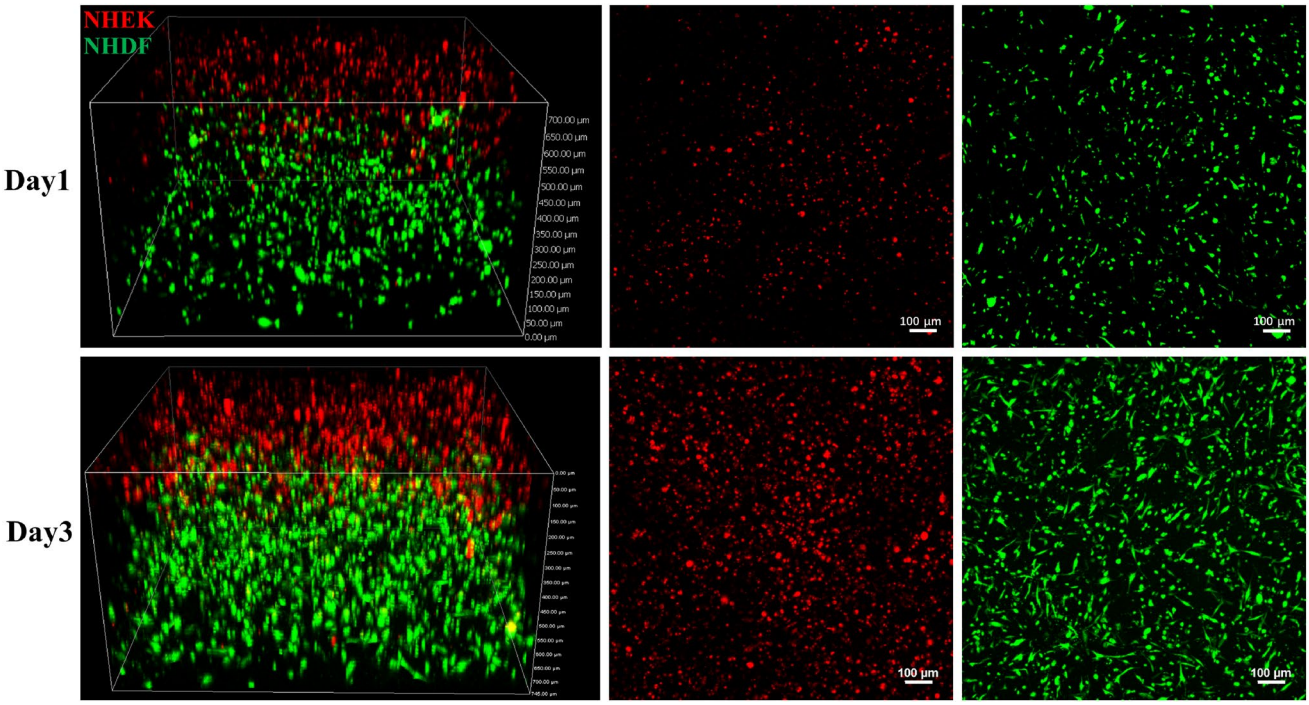

Fig. 12 Morphology and distribution of NHDFs and NHEKs in bi-layer skin (scale bar: 100 μm)

three days. The morphology and distribution of NHDFs and NHEKs in the bi-layer skin are shown in Fig. 12. After one day, the bi-layer skin maintained clear stratification with the limited spreading of fibroblasts. After 3 days, clear stratification was still observed with significant proliferation of fibroblasts and keratinocytes and increased spreading of fibroblasts. The survival and proliferation of cells in printed skin are central to the reconstruction of functional skin. The current results present a hydrogel with properties conducive to the growth and proliferation of dermal and epidermal cells.

Collagen hydrogel has ligands and pore sizes suitable for cell attachment, stimulating spreading and proliferation. Proliferation of dermal cells in transplanted skin facilitates epithelialization of the wound, accelerating closure. The degradation ratio of transplanted skin should match the skin regeneration ratio to support the early stage of skin reconstruction and provide space for re-growth in later stages. The directional arrangement of myofibroblasts is responsible for skin contraction and scarring but this consequence can be avoided by choice of appropriate pore size within the hydrogel.

4 Conclusion

The current study prepared and analyzed the properties, including the swelling, degradability, mechanical properties, microstructure and biological properties of Col/SA hydrogels with differing content of collagen and sodium alginate. With increasing sodium alginate content, the swelling ratio, degradation ratio, tensile modulus and compression modulus increased, while pore size, tensile elongation at break and biological activity decreased. With increasing collagen content, the swelling ratio, tensile modulus, compression modulus and tensile elongation at break increased, while degradation ratio, pore size and biological activity decreased. Hydrogels with 1% collagen content showed biological properties, micropores and degradation properties suitable for cell growth and skin wound healing. The 1% collagen hydrogel was shown to be a suitable bioink for biofabrication of a bi-layer skin construct. Fibroblasts and keratinocytes spread and proliferated in the bi-layer skin. Thus, the 1% collagen hydrogel shows good mechanical stability and promising properties for bioprinting of a skin model to be used in future wound healing research applications.

Acknowledgements This research was funded by the National Key R&D Program of China (2018YFE0207900), and People's Liberation Army (BWS17J036, 18-163-13-ZT-003-011-01) and the National Natural Science Foundation of China (51835010 and 51375371), and Xi'an Science and Technology Plan Project (21ZCZZHXJS-QCY6-0012).

Shaanxi Science and Technology Project (2022KXJ-147). Thanks to Shi Changquan and Yang Chuncheng of Shaanxi Ketao-AM Technology Co., Ltd. for their technical support for printing equipment.

Data Availability Statement The data and materials that support the findings of this study are available from the corresponding author upon reasonable request.

Declarations

Conflict of Interest The authors declare that they have no conflict of interest.

References

1. Weng, T. T., Zhang, W., Xia, Y. L., Wu, P., Yang, M., Jin, R. H., Xia, S. Z., Wang, J. L., You, C. L., Han, C. M., & Wang, X. G. (2021). 3D bioprinting for skin tissue engineering: Current status and perspectives. *Journal of Tissue Engineering, 12*, 20417314211028576. https://doi.org/10.1177/20417314211028574
2. Hosseini, M., & Shafiee, A. (2021). Engineering bioactive scaffolds for skin regeneration. *Small (Weinheim an der Bergstrasse, Germany), 17*, 2101384. https://doi.org/10.1002/smll.202101384
3. Zidaric, T., Milojevic, M., Gradisnik, L., Kleinschek, K. S., Maver, U., & Maver, T. (2020). Polysaccharide-based bioink formulation for 3D bioprinting of an in vitro model of the human dermis. *Nanomaterials, 10*, 733. https://doi.org/10.3390/nano10040733
4. Zhang, X., Yao, D., Zhao, W. Y., Zhang, R., Yu, B. R., Ma, G. P., Li, Y., Hao, D. F., & Xu, F. J. (2020). Engineering platelet-rich plasma based dual-network hydrogel as a bioactive wound dressing with potential clinical translational value. *Advanced Functional Materials, 31*, 2009258. https://doi.org/10.1002/adfm.202009258
5. Tavakoli, S., & Klar, A. S. (2021). Bioengineered skin substitutes: Advances and future trends. *Applied Sciences, 11*, 1493. https://doi.org/10.3390/app11041493
6. Tottoli, E. M., Dorati, R., Genta, I., Chiesa, E., Pisani, S., & Conti, B. (2020). Skin wound healing process and new emerging technologies for skin wound care and regeneration. *Pharmaceutics, 12*, 735. https://doi.org/10.3390/pharmaceutics12080735
7. Lian, Q., Jiao, T., Zhao, T. Z., Wang, H. C., Yang, S. M., & Li, D. C. (2021). 3D bioprinted skin substitutes for accelerated wound healing and reduced scar. *Journal of Bionic Engineering, 18*, 900–914. https://doi.org/10.1007/s42235-021-0053-8
8. Liu, T., Qiu, C., Ben, C., Li, H. H., & Zhu, S. H. (2019). One-step approach for full-thickness skin defect reconstruction in rats using minced split-thickness skin grafts with Pelnac overlay. *Burns Trauma, 7*, 19. https://doi.org/10.1186/s41038-019-0157-0
9. Mohamed Haflah, N. H., Ng, M. H., Mohd Yunus, M. H., Naicker, A. S., Htwe, O., Abdul Razak, K. A., & Idrus, R. (2018). Massive traumatic skin defect successfully treated with autologous, bilayered, tissue-engineered myderm skin substitute. *JBJS Case Connector, 8*, e38. https://doi.org/10.2106/JBJS.CC.17.00250
10. Varkey, M., Visscher, D. O., van Zuijlen, P. P. M., Atala, A., & Yoo, J. J. (2019). Skin bioprinting: the future of burn wound reconstruction? *Burns & Trauma, 7*, 4. https://doi.org/10.1186/S41038-019-0142-7
11. Jin, R. H., Cui, Y. C., Chen, H. J., Zhang, Z. Z., Weng, T. T., Xia, S. Z., Yu, M. R., Zhang, W., Shao, J. M., Yang, M., Han, C. M., & Wang, X. G. (2021). Three-dimensional bioprinting of a full-thickness functional skin model using acellular dermal matrix and gelatin methacrylamide bioink. *Acta Biomaterialia, 131*, 248–261. https://doi.org/10.1016/j.actbio.2021.07.012
12. Xu, J., Zheng, S. S., Hu, X. Y., Li, L. Y., Li, W. F., Parungao, R., Wang, Y. W., Nie, Y., Liu, T. Q., & Song, K. D. (2020). Advances in the research of bioinks based on natural collagen, polysaccharide and their derivatives for skin 3D bioprinting. *Polymers, 12*, 1237. https://doi.org/10.3390/polym12061237
13. Jakus, A. E., Rutz, A. L., & Shah, R. N. (2016). Advancing the field of 3D biomaterial printing. *Biomedical Materials, 11*, 014102. https://doi.org/10.1088/1748-6041/11/1/014102
14. Zhao, G. R., Cui, R. W., Chen, Y., Zhou, S. J., Wang, C., Hu, Z. M., Zheng, X. K., Li, M. H., & Qu, S. X. (2020). 3D Printing of well dispersed electrospun PLGA fiber toughened calcium phosphate scaffolds for osteoanagenesis. *Journal of Bionic Engineering, 17*, 652–668. https://doi.org/10.1007/s42235-020-0051-2
15. Yao, B., Wang, R., Wang, Y. H., Zhang, Y. J., Hu, T., Song, W., Li, Z., Huang, S., & Fu, X. B. (2020). Biochemical and structural cues of 3D-printed matrix synergistically direct MSC differentiation for functional sweat gland regeneration. *Science Advances, 6*, eaaz1094.
16. Zhou, F. F., Hong, Y., Liang, R. J., Zhang, X., Liao, Y. G., Jiang, D. M., Zhang, J. Y., Sheng, Z. X., Xie, C., Peng, Z., Zhuang, X. H., Bunpetch, V., Zou, Y. W., Huang, W. W., Zhang, Q., Alakpa, E. V., Zhang, S. F., & Ouyang, H. W. (2020). Rapid printing of bio-inspired 3D tissue constructs for skin regeneration. *Biomaterials, 258*, 120287. https://doi.org/10.1016/j.biomaterials.2020.120287
17. Lee, W., Debasitis, J. C., Lee, V. K., Lee, J. H., Fischer, K., Edminster, K., Park, J. K., & Yoo, S. S. (2009). Multi-layered culture of human skin fibroblasts and keratinocytes through three-dimensional freeform fabrication. *Biomaterials, 30*, 1587–1595. https://doi.org/10.1016/j.biomaterials.2008.12.009
18. Koch, L., Deiwick, A., Schlie, S., Michael, S., Gruene, M., Coger, V., Zychlinski, D., Schambach, A., Reimers, K., Vogt, P. M., & Chichkov, B. (2012). Skin tissue generation by laser cell printing. *Biotechnology and Bioengineering, 109*, 1855–1863. https://doi.org/10.1002/bit.24455
19. Lee, V., Singh, G., Trasatti, J. P., Bjornsson, C., Xu, X. W., Tran, T. N., Yoo, S. S., Dai, G. H., & Karande, P. (2014). Design and fabrication of human skin by three-dimensional bioprinting. *Tissue Engineering: Part C, 20*, 473–484. https://doi.org/10.1089/ten.tec.2013.0335
20. Pereira, R. F., Barrias, C. C., Bártolo, P. J., & Granja, P. L. (2018). Cell-instructive pectin hydrogels crosslinked via thiol-norbornene photo-click chemistry for skin tissue engineering. *Acta Biomaterialia, 66*, 282–293. https://doi.org/10.1016/j.actbio.2017.11.016
21. Kim, B. S., Ahn, M., Cho, W. W., Gao, G., Jang, J., & Cho, D. W. (2021). Engineering of diseased human skin equivalent using 3D cell printing for representing pathophysiological hallmarks of type 2 diabetes in vitro. *Biomaterials, 272*, 120776. https://doi.org/10.1016/j.biomaterials.2021.120776
22. Kim, G. H., Ahn, S., Kim, Y. Y., Cho, Y., & Chun, W. (2011). Coaxial structured collagen-alginate scaffolds: fabrication, physical properties, and biomedical application for skin tissue regeneration. *Journal of Materials Chemistry, 21*, 6165–6172. https://doi.org/10.1039/c0jm03452e
23. Park, J. A., Lee, H. R., Park, S. Y., & Jung, S. (2020). Self-organization of fibroblast-laden 3D collagen microstructures from inkjet-printed cell patterns. *Advanced Biosystems, 4*, 1900280. https://doi.org/10.1002/adbi.201900280
24. Shi, L., Xiong, L. M., Hu, Y. Q., Li, W. C., Chen, Z. C., Liu, K., & Zhang, X. L. (2018). Three-dimensional printing alginate/gelatin scaffolds as dermal substitutes for skin tissue engineering. *Polymer Engineering & Science, 58*, 1782–1790. https://doi.org/10.1002/pen.24779

25. Kim, B. S., Kwon, Y. W., Kong, J. S., Park, G. T., Gao, G., Han, W., Kim, M. B., Lee, H., Kim, J. H., & Cho, D. W. (2018). 3D cell printing of in vitro stabilized skin model and in vivo pre-vascularized skin patch using tissue-specific extracellular matrix bioink: A step towards advanced skin tissue engineering. *Biomaterials, 168*, 38–53. https://doi.org/10.1016/j.biomaterials.2018.03.040
26. Admane, P., Gupta, A. C., Jois, P., Roy, S., Lakshmanan, C. C., Kalsi, G., Bandyopadhyay, B., & Ghosh, S. (2019). Direct 3D bioprinted full-thickness skin constructs recapitulate regulatory signaling pathways and physiology of human skin. *Bioprinting, 15*, e00051. https://doi.org/10.1016/j.bprint.2019.e00051
27. Pourchet, L. J., Thepot, A., Albouy, M., Courtial, E. J., Boher, A., Blum, L. J., & Marquette, C. A. (2017). Human skin 3D bioprinting using scaffold-free approach. *Advanced Healthcare Materials, 6*, 1601101. https://doi.org/10.1002/adhm.201601101
28. Cubo, N., Garcia, M., Canizo, J. F. D., Velasco, D., & Jorcano, J. L. (2017). 3D bioprinting of functional human skin: production and in vivo analysis. *Biofabrication, 9*, 015006. https://doi.org/10.1088/1758-5090/9/1/015006
29. Derr, K., Zou, J., Luo, K., Song, M. J., Sittampalam, G. S., Zhou, C., Michael, S., Ferrer, M., & Derr, P. (2019). Fully three-dimensional bioprinted skin equivalent constructs with validated morphology and barrier function. *Tissue Engineering: Part C, 25*, 334–343. https://doi.org/10.1089/ten.tec.2018.0318
30. Kim, B. S., Gao, G., Kim, J. Y., & Cho, D. W. (2018). 3D cell printing of perfusable vascularized human skin equivalent composed of epidermis, dermis, and hypodermis for better structural recapitulation of native skin. *Advanced Healthcare Materials, 8*, 1801019. https://doi.org/10.1002/adhm.201801019
31. Jorgensen, A. M., Varkey, M., Gorkun, A., Clouse, C., Xu, L., Chou, Z., Murphy, S., Molnar, J., Lee, S. J., Yoo, J. J., Soker, S., & Atala, A. (2020). Bioprinted skin recapitulates normal collagen remodeling in full-thickness wounds. *Tissue Engineering: Part A, 26*, 512–526. https://doi.org/10.1089/ten.tea.2019.0319
32. Kim, B. S., Lee, J. S., Gao, G., & Cho, D. W. (2017). Direct 3D cell-printing of human skin with functional transwell system. *Biofabrication, 9*, 025034. https://doi.org/10.1088/1758-5090/aa71c8
33. Albanna, M., Binder, K. W., Murphy, S. V., Kim, J., Qasem, S. A., Zhao, W. X., Tan, J., El-Amin, I. B., Dice, D. D., Marco, J., Green, J., Xu, T., Skardal, A., Holmes, J. H., Jackson, J. D., Atala, A., & Yoo, J. J. (2019). In situ bioprinting of autologous skin cells accelerates wound healing of extensive excisional full-thickness wounds. *Scientific Reports, 9*, 1856. https://doi.org/10.1038/S41598-018-38366-W
34. Liu, X., Michael, S., Bharti, K., Ferrer, M., & Song, M. J. (2020). A biofabricated vascularized skin model of atopic dermatitis for preclinical studies. *Biofabrication, 12*, 035002. https://doi.org/10.1088/1758-5090/ab76a1
35. Baltazar, T., Merola, J., Catarino, C. M., Xie, C. B., Kirkiles-Smith, N., Lee, V., Hotta, S. Y. K., Dai, G., Xu, X., Ferreira, F. C., Saltzman, W. M., Pober, J. S., & Karande, P. (2019). Three dimensional bioprinting of a vascularized and perfusable skin graft using human keratinocytes, fibroblasts, pericytes, and endothelial cells. *Tissue Engineering: Part A, 26*, 227–238. https://doi.org/10.1089/ten.tea.2019.0201
36. Ng, W. L., Qi, J. T. Z., Yeong, W. Y., & Naing, M. W. (2018). Proof-of-concept: 3D bioprinting of pigmented human skin constructs. *Biofabrication, 10*, 025005. https://doi.org/10.1088/1758-5090/aa9e1e
37. Min, D., Lee, W., Bae, I. H., Lee, T. R., Croce, P., & Yoo, S. S. (2017). Bioprinting of biomimetic skin containing melanocytes. *Experimental Dermatology, 27*, 453–459. https://doi.org/10.1111/exd.13376
38. DeBruler, D. M., Zbinden, J. C., Baumann, M. E., Blackstone, B. N., Malara, M. M., Bailey, J. K., Supp, D. M., & Powell, H. M. (2018). Early cessation of pressure garment therapy results in scar contraction and thickening. *PLoS ONE, 13*, e0197558. https://doi.org/10.1371/journal.pone.0197558
39. Yoon, H., Lee, J. S., Yim, H., Kim, G., & Chun, W. (2016). Development of cell-laden 3D scaffolds for efficient engineered skin substitutes by collagen gelation. *RSC Advances, 6*, 21439–21447. https://doi.org/10.1039/c5ra19532b
40. Cheng, R. Y., Eylert, G., Gariepy, J. M., He, S., Ahmad, H., Gao, Y., Priore, S., Hakimi, N., Jeschke, M. G., & Gunther, A. (2020). Handheld instrument for wound-conformal delivery of skin precursor sheets improves healing in full-thickness burns. *Biofabrication, 12*, 025002. https://doi.org/10.1088/1758-5090/ab6413
41. Wang, R., Wang, Y. H., Yao, B., Hu, T., Li, Z., Huang, S., & Fu, X. B. (2019). Beyond 2D: 3D bioprinting for skin regeneration. *International Wound Journal, 16*, 134–138. https://doi.org/10.1111/iwj.13003
42. Chouhan, D., Dey, N., Bhardwaj, N., & Mandal, B. B. (2019). Emerging and innovative approaches for wound healing and skin regeneration: Current status and advances. *Biomaterials, 216*, 119267. https://doi.org/10.1016/j.biomaterials.2019.119267
43. Yannas, I. V., Tzeranis, D., & So, P. T. (2015). Surface biology of collagen scaffold explains blocking of wound contraction and regeneration of skin and peripheral nerves. *Biomedical Materials, 11*, 014106. https://doi.org/10.1088/1748-6041/11/1/014106
44. Yannas, I. V., Tzeranis, D. S., & So, P. T. C. (2017). Regeneration of injured skin and peripheral nerves requires control of wound contraction, not scar formation. *Wound Repair and Regeneration, 25*, 177–191. https://doi.org/10.1111/wrr.12516
45. Yannas, I. V., Tzeranis, D. S., & So, P. T. C. (2018). Regeneration mechanism for skin and peripheral nerves clarified at the organ and molecular scales. *Current Opinion in Biomedical Engineering, 6*, 1–7. https://doi.org/10.1016/j.cobme.2017.12.002
46. Perez-Valle, A., Del Amo, C., & Andia, I. (2020). Overview of current advances in extrusion bioprinting for skin applications. *International Journal of Molecular Sciences, 21*, 6679. https://doi.org/10.3390/ijms21186679
47. Vanaei, S., Parizi, M. S., Vanaei, S., Salemizadehparizi, F., & Vanaei, H. R. (2021). An overview on materials and techniques in 3D bioprinting toward biomedical application. *Engineered Regeneration, 2*, 1–18. https://doi.org/10.1016/j.engreg.2020.12.001
48. Gibney, R., Patterson, J., & Ferraris, E. (2021). High-resolution bioprinting of recombinant human collagen type III. *Polymers, 13*, 2973. https://doi.org/10.3390/polym13172973
49. Wang, L., Shelton, R. M., Cooper, P. R., Lawson, M., Triffitt, J. T., & Barralet, J. E. (2003). Evaluation of sodium alginate for bone marrow cell tissue engineering. *Biomaterials, 24*, 3475–3481. https://doi.org/10.1016/s0142-9612(03)00167-4
50. Kollman, J. M., Pandi, L., Sawaya, M. R., Riley, M., & Doolittle, R. F. (2009). Crystal structure of human fibrinogen. *Biochemistry, 48*, 3877–3886. https://doi.org/10.1021/bi802205g
51. Kaijzel, E. L., Koolwijk, P., Erck, M. G. M. V., Hinsbergh, V. W. M. V., & Maat, M. P. M. D. (2006). Molecular weight fibrinogen variants determine angiogenesis rate in a fibrin matrix in vitro and in vivo. *Journal of Thrombosis and Haemostasis, 4*, 1975–7981.
52. Rittié, L. (2017). Type I collagen purification from rat tail tendons. *Methods in Molecular Biology, 1627*, 287–308. https://doi.org/10.1007/978-1-4939-7113-8_19
53. Amirian, J., Zeng, Y., Shekh, M. I., Sharma, G., Stadler, F. J., Song, J., Du, B., & Zhu, Y. (2021). In-situ crosslinked hydrogel based on amidated pectin/oxidized chitosan as potential wound dressing for skin repairing. *Carbohydrate Polymers, 251*, 117005. https://doi.org/10.1016/j.carbpol.2020.117005
54. Zhang, Y., Chen, H. G., Li, Y. L., Fang, A., Wu, T. F., Shen, C. Y., Zhao, Y. Y., & Zhang, G. Z. (2020). A transparent sericin-polyacrylamide interpenetrating network hydrogel as visualized dressing material. *Polymer Testing, 87*, 106517. https://doi.org/10.1016/j.polymertesting.2020.106517

55. Bulcke, A. I. V. D., Bogdanov, B., Rooze, N. D., Schacht, E. H., Cornelissen, M., & Berghmans, H. (2000). Structural and rheological properties of methacrylamide modified gelatin hydrogels. *Biomacromolecules, 1*, 31–38.
56. Raafat, A. I., El-Sawy, N. M., Badawy, N. A., Mousa, E. A., & Mohamed, A. M. (2018). Radiation fabrication of Xanthan-based wound dressing hydrogels embedded ZnO nanoparticles: In vitro evaluation. *International Journal of Biological Macromolecules, 118*, 1892–1902. https://doi.org/10.1016/j.ijbiomac.2018.07.031
57. Shefa, A. A., Amirian, J., Kang, H. J., Bae, S. H., Jung, H. I., Choi, H. J., Lee, S. Y., & Lee, B. T. (2017). In vitro and in vivo evaluation of effectiveness of a novel TEMPO-oxidized cellulose nanofiber-silk fibroin scaffold in wound healing. *Carbohydrate Polymers, 177*, 284–296. https://doi.org/10.1016/j.carbpol.2017.08.130
58. Liu, J., Li, J., Yu, F., Zhao, Y. X., Mo, X. M., & Pan, J. F. (2020). In situ forming hydrogel of natural polysaccharides through schiff base reaction for soft tissue adhesive and hemostasis. *International Journal of Biological Macromolecules, 147*, 653–666. https://doi.org/10.1016/j.ijbiomac.2020.01.005
59. Brown, B. N., & Badylak, S. F. (2014). Biocompatibility and immune response to biomaterials. *Regenerative Medicine Applications in Organ Transplantation, 11*, 151–162. https://doi.org/10.1016/b978-0-12-398523-1.00011-2
60. Beiki, B., Zeynali, B., & Seyedjafari, E. (2017). Fabrication of a three dimensional spongy scaffold using human Wharton's jelly derived extra cellular matrix for wound healing. *Materials Science and Engineering: C, 78*, 627–638. https://doi.org/10.1016/j.msec.2017.04.074
61. Li, H. J., Tan, Y. J., Leong, K. F., & Li, L. (2017). 3D bioprinting of highly thixotropic alginate/methylcellulose hydrogel with strong interface bonding. *ACS Applied Materials & Interfaces, 9*, 20086–20097. https://doi.org/10.1021/acsami.7b04216
62. Yoon, S., Park, J. A., Lee, H. R., Yoon, W. H., Hwang, D. S., & Jung, S. (2018). Inkjet-spray hybrid printing for 3D freeform fabrication of multilayered hydrogel structures. *Advanced Healthcare Materials, 7*, 1800050. https://doi.org/10.1002/adhm.201800050
63. Labroo, P., Irvin, J., Johnson, J., Sieverts, M., Miess, J., Robinson, I., Baetz, N., Garrett, C., & Sopko, N. (2020). Physical characterization of swine and human skin: Correlations between Raman spectroscopy, Tensile testing, Atomic force microscopy (AFM), Scanning electron microscopy (SEM), and Multiphoton microscopy (MPM). *Skin Research and Technology, 27*, 501–510. https://doi.org/10.1111/srt.12976
64. Osidak, E. O., Karalkin, P. A., Osidak, M. S., Parfenov, V. A., Sivogrivov, D. E., Pereira, F. D. A. S., Gryadunova, A. A., Koudan, E. V., Khesuani, Y. D., Kasyanov, V. A., Belousov, S. I., Krasheninnikov, S. V., Grigoriev, T. E., Chvalun, S. N., Bulanova, E. A., Mironov, V. A., & Domogatsky, S. P. (2019). Viscoll collagen solution as a novel bioink for direct 3D bioprinting. *Journal of Materials Science: Materials in Medicine, 30*, 31. https://doi.org/10.1007/s10856-019-6233-y
65. Govindharaj, M., Roopavath, U. K., & Rath, S. N. (2019). Valorization of discarded Marine Eel fish skin for collagen extraction as a 3D printable blue biomaterial for tissue engineering. *Journal of Cleaner Production, 230*, 412–419. https://doi.org/10.1016/j.jclepro.2019.05.082